

Validation of acoustic-analogy predictions for sound radiated by turbulence

Julia Whitmire and Sutanu Sarkar

Citation: *Physics of Fluids* (1994-present) **12**, 381 (2000); doi: 10.1063/1.870316

View online: <http://dx.doi.org/10.1063/1.870316>

View Table of Contents: <http://scitation.aip.org/content/aip/journal/pof2/12/2?ver=pdfcov>

Published by the [AIP Publishing](#)

Articles you may be interested in

[Comparison of sound power radiation from isolated airfoils and cascades in a turbulent flow](#)

J. Acoust. Soc. Am. **129**, 3521 (2011); 10.1121/1.3569706

[Scattering of an entropy disturbance into sound by a symmetric thin body](#)

Phys. Fluids **21**, 096101 (2009); 10.1063/1.3225143

[A computational method of evaluating noncompact sound based on vortex sound theory](#)

J. Acoust. Soc. Am. **121**, 1353 (2007); 10.1121/1.2431345

[Sound transmission across a smooth nonuniform section in an infinitely long duct](#)

J. Acoust. Soc. Am. **112**, 2602 (2002); 10.1121/1.1512699

[Broadband sound generation by confined turbulent jets](#)

J. Acoust. Soc. Am. **112**, 677 (2002); 10.1121/1.1492817



Validation of acoustic-analogy predictions for sound radiated by turbulence

Julia Whitmire and Sutanu Sarkar

Mechanical and Aerospace Engineering, University of California, San Diego, California 92093

(Received 7 July 1998; accepted 5 October 1999)

Predicting sound radiated by turbulence is of interest in aeroacoustics, hydroacoustics, and combustion noise. Significant improvements in computer technology have renewed interest in applying numerical techniques to predict sound from turbulent flows. One such technique is a hybrid approach in which the turbulence is computed using a method such as direct numerical simulation (DNS) or large eddy simulation (LES), and the sound is calculated using an acoustic analogy. In this study, sound from a turbulent flow is computed using DNS, and the DNS results are compared with acoustic-analogy predictions for mutual validation. The source considered is a three-dimensional region of forced turbulence which has limited extent in one coordinate direction and is periodic in the other two directions. Sound propagates statistically as a plane wave from the turbulence to the far field. The cases considered here have a small turbulent Mach number so that the source is spatially compact; that is, the turbulence integral scale is much smaller than the acoustic wavelength. The scaling of the amplitude and frequency of the far-field sound for the problem considered are derived in an analysis based on Lighthill's acoustic analogy. The analytical results predict that the far-field sound should exhibit "dipole-type" behavior; the root-mean-square pressure in the acoustic far field should increase as the cube of the turbulent Mach number. The acoustic power normalized by the turbulent dissipation rate is also predicted to scale as turbulent Mach number cubed. Agreement between the DNS results and the acoustic-analogy predictions is good. This study verifies the ability of the Lighthill acoustic analogy to predict sound generated by a three-dimensional, turbulent source containing many length and time scales. © 2000 American Institute of Physics. [S1070-6631(00)02501-0]

I. INTRODUCTION

A fundamental concern in aeroacoustics is the prediction of the far-field sound radiated by turbulence. Advanced numerical methods for this purpose have received attention recently. Computing the far-field sound by DNS (direct numerical simulation) on a very large computational domain which includes both the turbulent source and the acoustic far field is unfortunately very expensive and problematic for even relatively simple flows. An alternative strategy is to calculate the sound using a hybrid approach in which the turbulence is computed using a method such as DNS or LES (large eddy simulation), and the far-field sound is calculated using an acoustic analogy. Application of the hybrid approach requires understanding and accurately capturing the behavior of the dominant acoustic sources in a particular flow. Invalid approximations to the source term in the acoustic analogy can lead to large errors in the predicted sound.¹ The objective of this study is to evaluate the hybrid approach for predicting sound from broadband turbulence at low turbulent Mach number using the Lighthill acoustic analogy.

Lighthill² introduces the idea of calculating the far-field sound generated by unsteady flow with an acoustic analogy. In Lighthill's analogy, the fully nonlinear problem is taken to be analogous to the problem of sound propagation in a linear acoustic medium at rest subject to an external forcing that represents the turbulent source. Starting with Lighthill's

acoustic analogy, Proudman³ derives an equation for the radiated acoustic power per unit mass of the turbulence, $P = \alpha \epsilon M_t^5$. Here ϵ is the mean rate of turbulent energy dissipation per unit mass, M_t is the turbulent Mach number, and the Proudman constant, α , is of order 10. In Proudman's analysis, the equation for α is derived assuming Gaussian statistics with normal joint probability distributions for the turbulent velocities and their first two time derivatives.

The following studies use the hybrid approach to calculate the sound from turbulence and compare acoustic-analogy predictions with theoretical and experimental results. Sarkar and Hussaini⁴ compute the sound from decaying isotropic turbulence using a hybrid DNS/Lighthill acoustic-analogy approach. Witkowska *et al.*⁵ also compute the sound from isotropic turbulence for forced and unforced cases using both DNS and LES to evaluate the turbulent source in the Lighthill acoustic analogy. These simulations of isotropic turbulence have periodic boundary conditions in all directions. Since there is no far field in these simulations, the radiated sound cannot be computed directly; however, the statistics of the source term in the acoustic analogy can be obtained. Lilley⁶ derives an alternative analytical method of determining α and evaluates his analytical results using statistics of the Lighthill source obtained from the DNS databases of Sarkar and Hussaini⁴ and Dubois.⁷ These studies all show that the hybrid acoustic-analogy method is a feasible approach in that DNS/LES can be used to compute the

acoustic source and thereby obtain sound radiated by isotropic turbulence.

Studies have also been performed to validate various forms of the acoustic analogy for different flow configurations by comparing the sound calculated from direct computations or exact analytical solutions with acoustic-analogy predictions. The emphasis in almost all of these studies is to investigate the sound from large coherent structures rather than the effects of smaller turbulence scales on the radiated sound. Mitchell, Lele, and Moin⁸ and Colonius, Lele, and Moin⁹ study the sound radiated by a compressible co-rotating vortex pair and the scattering of sound waves from a compressible viscous vortex, respectively. Colonius, Moin, and Lele¹⁰ validate the Lilley acoustic analogy for a forced, two-dimensional, compressible shear layer by comparing DNS results with acoustic-analogy predictions. The flow studied by Colonius *et al.*¹⁰ is not turbulent. Vortex roll-up and pairing occur at fixed locations (stationary acoustic sources), and the sound is dominated by these forced vortex dynamics. Mitchell, Lele, and Moin¹¹ validate the Lighthill acoustic analogy by comparison with DNS results for axisymmetric, nonturbulent subsonic and supersonic jets. As in the study by Colonius *et al.*,¹⁰ the only acoustic sources considered are the large coherent structures considered to be the dominant acoustic sources in supersonic jets.

In recent work, Bastin *et al.*¹² calculate the sound from a subsonic turbulent plane jet using the hybrid approach. In this work, the jet flow is computed using semideterministic modeling (SDM), and the far-field sound is predicted using Lighthill's acoustic analogy. As discussed by Bastin *et al.*, a problem with SDM for this application is that only the large coherent structures are computed; the smaller acoustically active scales of the turbulence are unresolved. Freund¹³ performs a DNS of a jet with Mach number 0.9 and Reynolds number 3600 and analyzes the acoustic sources in the jet. In Freund's work, the Lighthill source is computed from the DNS results using Fourier methods.

The objective of this study is to validate the Lighthill acoustic analogy by comparison with a direct computation of far-field sound for a three-dimensional, turbulent flow. Validation using experimental results is problematic since the equivalent acoustic source in a turbulent flow is difficult to characterize completely and includes significant contributions from multipoles of different orders that invalidate simple scaling laws for the acoustic power and spectra. The approach in this study is to devise a problem in which the equivalent acoustic source has well-defined properties, derive scaling laws for the radiated sound using the acoustic analogy, compute the sound in a full DNS on a large domain which includes the turbulence and extends to the acoustic far field, and validate acoustic-analogy predictions by comparison with DNS results. Unlike previous simulations^{4,5} of sound radiated by isotropic turbulence, a nonperiodic direction is allowed so that the far-field sound radiating in that direction can be explicitly computed in the DNS.

The source is a three-dimensional region of forced turbulence which is periodic in the x and z directions and has limited extent in the y direction. The turbulence is embedded in a large domain otherwise at ambient conditions. The do-

main extends to the acoustic far field. Since the source has finite extent only in the y direction, acoustic wave propagation is statistically one-dimensional. The plane-mean sound propagates from the turbulence to the far field in the y direction. Here plane-mean quantities are defined as $\langle \cdot \rangle = (1/A_{xz}) \int_{A_{xz}} (\cdot) dx dz$, where A_{xz} is the cross-sectional area normal to the y direction. There is no far field in the x or z directions. The turbulence is forced in time to prevent the rapid decay of the plane-mean sound seen in the case where the source is a region of decaying isotropic turbulence. The forcing is accomplished without introducing fluctuating dilatation.

Full DNS are performed for two cases with $M_t \ll 1$. Here M_t is the turbulent Mach number. Using the Lighthill acoustic analogy, the scaling of the amplitude of the plane-mean sound with turbulent Mach number is derived. Analytical results predict that the amplitude of the plane-mean sound should scale with turbulent Mach number as sound from a distribution of dipoles. The turbulence in the problem considered is a dipole-type source. The "quadrupole-type" behavior derived by Lighthill for a region of turbulence limited in extent in all three coordinate directions does not apply in this problem since the turbulence has limited extent only in a single direction. These analytical results are derived in Sec. II. Numerical techniques used in the DNS are discussed in Sec. III. In Sec. IV, the DNS results are discussed and compared with acoustic-analogy predictions. Conclusions are given in Sec. V.

II. ANALYTICAL RESULTS

A. Derivation

For a region of unsteady flow in free space which is limited in extent in all three coordinate directions, Lighthill derives

$$\frac{\partial^2 \rho'}{\partial t^2} - c_0^2 \nabla^2 \rho' = \frac{\partial^2 T_{ij}}{\partial x_i \partial x_j}, \quad (1)$$

where the Lighthill stress tensor, $T_{ij} = (\rho u_i u_j) - \tau_{ij} + (p' - c_0^2 \rho') \delta_{ij}$ is the difference between stresses in the real flow and stresses in the uniform acoustic medium at rest. Here ρ is the density, $\mathbf{u} = (u, v, w)$ is the unsteady source velocity, c_0 is the ambient sound speed, and

$$\tau_{ij} = 2\mu \left(e_{ij} - \frac{1}{3} e_{kk} \delta_{ij} \right) = \mu \left(\frac{\partial u_i}{\partial x_j} + \frac{\partial u_j}{\partial x_i} \right) - \frac{2}{3} \mu \frac{\partial u_k}{\partial x_k} \delta_{ij}, \quad (2)$$

is the viscous stress tensor. In Eq. (2), μ is the dynamic viscosity, e_{ij} is the rate of strain tensor, and e_{kk} is the divergence of the velocity field. The superscript prime notation denotes fluctuations relative to the ambient quantity. Equation (1) is exact for an arbitrary fluid motion. Assuming negligible viscous stresses and heat transfer between regions inside and outside the flow and low turbulent Mach number, the term T_{ij} can be approximated as $T_{ij} \sim \rho_0 (u_i u_j)$, where ρ_0 is the ambient density. For the case with no mean flow, $T_{ij} \sim \rho_0 u'_i u'_j$.

For a source periodic in the x and z directions and limited in extent in the y direction, Eq. (1) is plane averaged to give

$$\frac{\partial^2 \langle \rho \rangle'}{\partial t^2} - c_0^2 \frac{d^2 \langle \rho \rangle'}{dy^2} = \langle T \rangle'. \quad (3)$$

Here $\langle \cdot \rangle'$ denotes averages in the xz plane, and $T' = \rho_0 \partial^2 (u'_i u'_j) / \partial x_i \partial x_j$. Taking Fourier transforms in time, Eq. (3) becomes

$$\frac{d^2 \widehat{\langle \rho \rangle'}}{dy^2} + k_A^2 \widehat{\langle \rho \rangle'} = - \frac{\widehat{\langle T \rangle'}}{c_0^2}, \quad (4)$$

where $\widehat{\langle \rho \rangle'}(y, \omega)$ and $\widehat{\langle T \rangle'}(y, \omega)$ are the Fourier transforms of $\langle \rho \rangle'$ and $\langle T \rangle'$, respectively, and $k_A = \omega/c_0$ is the acoustic wave number. Here the Fourier transform in time is defined by

$$\hat{f}(y, \omega) = \int f(y, t) e^{i\omega t} dt \quad (5)$$

and

$$f(y, t) = \frac{1}{2\pi} \int \hat{f}(y, \omega) e^{-i\omega t} d\omega. \quad (6)$$

The one-dimensional Green's function for Eq. (4) is

$$G(y, \xi) = \frac{1}{2ik_A} e^{ik_A|y-\xi|}, \quad (7)$$

so the solution to Eq. (4) is

$$\widehat{\langle \rho \rangle'}(y, \omega) = - \frac{1}{2ik_A c_0^2} \int e^{ik_A|y-\xi|} \widehat{\langle T \rangle'}(\xi, \omega) d\xi. \quad (8)$$

Retaining terms of $O(y^{-1})$ for sound in the far field

$$\widehat{\langle \rho \rangle'}(y, \omega) = - \frac{e^{ik_A y}}{2ik_A c_0^2} \int \widehat{\langle T \rangle'}(\xi, \omega) e^{-ik_A \xi} d\xi. \quad (9)$$

The integral in Eq. (9) is the Fourier transform in y of $\widehat{\langle T \rangle}'$ at frequency ω and wave number $-k_A$

$$\int \widehat{\langle T \rangle'}(\xi, \omega) e^{-ik_A \xi} d\xi = \widetilde{\langle T \rangle}'(k_y = -k_A, \omega). \quad (10)$$

Here the Fourier transform in both the y direction and time is defined by

$$\tilde{A}(k_y, \omega) = \int A(y, t) e^{i(k_y y + \omega t)} dy dt \quad (11)$$

and

$$A(y, t) = \frac{1}{2\pi} \int \tilde{A}(k_y, \omega) e^{-i(k_y y + \omega t)} dk_y d\omega. \quad (12)$$

Thus, for a given frequency ω , only wave numbers with $k_A = \omega/c_0$ in the source contribute to the far-field sound. This condition is required because the turbulence is limited in extent in the y direction; $\widehat{\langle T \rangle}'(y, \omega) \rightarrow 0$ for large y . Consequently, density fluctuations must satisfy the acoustic dispersion relationship in the far field.

In this problem, $\widehat{\langle T \rangle}' = \rho_0 \widehat{\langle u'_i u'_j \rangle}'$, ij is dominated by the term $\rho_0 \widehat{\langle v^2 \rangle}'_{,yy}$. Assuming $\widehat{\langle T \rangle}' \sim \rho_0 \widehat{\langle v^2 \rangle}'_{,yy}$, Eq. (9) becomes

$$\widehat{\langle \rho \rangle'}(y, \omega) = \frac{1}{2ik_A c_0^2} e^{i(\omega/6)y} \rho_0 k_A^2 \widehat{\langle v^2 \rangle}'(-k_A, \omega). \quad (13)$$

Taking the inverse Fourier transform in time of Eq. (13) gives

$$\frac{\langle \rho \rangle'(y, t)}{\rho_0} = - \frac{1}{4\pi c_0^3} \int e^{-i\omega[t-(y/c_0)]} i\omega \widehat{\langle v^2 \rangle}'(-k_A, \omega) d\omega. \quad (14)$$

Using

$$-i\omega \widehat{\langle v^2 \rangle}'(k_A, \omega) = \left\langle \frac{\partial v^2}{\partial t} \right\rangle'(-k_A, \omega), \quad (15)$$

in Eq. (14) and redefining $t - y/c_0$ to be the new variable t , where t is the retarded time, gives

$$\frac{\langle \rho \rangle'(y, t + y/c_0)}{\rho_0} = \frac{1}{4\pi c_0^3} \int e^{-i\omega t} \left\langle \frac{\partial v^2}{\partial t} \right\rangle'(-k_A, \omega) d\omega. \quad (16)$$

Equation (16) predicts the plane-mean sound radiated by a low-Mach-number turbulent source which is periodic in the x and z directions and limited in extent in the y direction. The far-field sound, $\langle p \rangle' = c_0^2 \langle \rho \rangle'$, is determined by the space-time characteristics of the term $\partial \langle v^2 \rangle' / \partial t$ in the turbulent source. In Eq. (16), the acoustic analogy is written in terms of time derivatives instead of space derivatives. Lighthill² advocates the use of the time-derivative form because the time delay, y/c_0 , between source emission and observer reception can be neglected in subsequent analysis.

For a low-Mach-number source, the change in acoustic wave number for two cases with different values of M_t is $\Delta k_A = k_{A2} - k_{A1} = \Delta \omega / c_0 = \Delta M_t \ll 1$. For $\Delta M_t \ll 1$, Eq. (16) gives

$$\frac{\langle \rho \rangle'(y, t + y/c_0)}{\rho_0} = O \left[\frac{l_T}{c_0^3} \left\langle \frac{\partial v^2}{\partial t} \right\rangle \right] = O \left[\frac{v_T^2 l_T}{c_0^3 t_T} \right] = O(M_t^3). \quad (17)$$

Here l_T , v_T , and $t_T \sim l_T / v_T$ are the characteristic turbulence length, velocity, and time scales, respectively, and $M_t \sim v_T / c_0$. In obtaining Eq. (17), a self-similar spectrum of $\langle \partial v^2 / \partial t \rangle$ with l_T and t_T is assumed.

B. Predicted scaling of source and sound frequency

For the DNS cases considered, the ratio of the frequency of the term $\partial \langle v^2 \rangle' / \partial t$ in the two DNS cases is given by

$$\omega_{Sr} = \frac{\omega_{S,1}}{\omega_{S,2}} = \frac{M_{t,1}}{M_{t,2}} = M_{tr}. \quad (18)$$

Since the acoustic analogy predicts that the source frequency, ω_A , is equal to ω_S , the acoustic frequency, for a spatially compact source, the acoustic frequencies in the two DNS cases are related by

$$\omega_{Ar} = \frac{\omega_{A,1}}{\omega_{A,2}} = \frac{M_{t,1}}{M_{t,2}} = M_{tr}. \quad (19)$$

Here the source turbulent Mach number ratio is $M_{tr} = M_{t,1}/M_{t,2}$. The subscripts 1 and 2 are used to denote values of variables for the two cases. Note that Eqs. (18) and (19) give the scaling of the source and sound frequency for the specific cases considered in the DNS with $l_{T1} = l_{T2}$ and $c_{01} = c_{02}$.

1. Predicted scaling of source and sound amplitude

For the spatially compact cases considered, the scaling of density fluctuations in the turbulence is obtained from the Poisson equation for the incompressible pressure

$$\nabla^2 p^{I'} = -\rho_0 u'_{i,j} u'_{j,i}. \quad (20)$$

Using Eq. (20) to estimate plane-mean density fluctuations in the turbulent source gives

$$\frac{\langle \rho \rangle'_S}{\rho_0} = O(M_t^2). \quad (21)$$

Using Eq. (17) to estimate plane-mean density fluctuations in the acoustic far field gives

$$\frac{\langle \rho \rangle'_A}{\rho_0} = O(M_t^3). \quad (22)$$

The results of our analysis predict that the plane-mean sound radiated by the turbulence in this problem is equivalent to sound from a distribution of *dipole* sources. The single time derivative on the right-hand-side of Eq. (16) is also indicative of a dipole-type source.

For the purpose of evaluating these scaling predictions, considering the statistics of the plane-mean dilatation fluctuations, $\langle d \rangle'$, is preferable to considering the statistics of the plane-mean density or pressure fluctuations because the low-frequency drift in the mean pressure complicates the computation of $\langle p \rangle'$ and $\langle \rho \rangle'$. A similar low-frequency drift in the far-field mean pressure was observed by Colonius *et al.*¹⁰ and Mitchell *et al.*¹¹ The plane-mean dilatation fluctuations are related to the plane-mean density fluctuations by

$$\widehat{\langle d \rangle'} = \frac{i\omega}{\rho_0} \widehat{\langle \rho \rangle'}. \quad (23)$$

From Eq. (21), in the turbulent source

$$\frac{\langle d \rangle'_S}{d_0} = O(M_t^3). \quad (24)$$

From Eq. (22), in the far field

$$\frac{\langle d \rangle'_A}{d_0} = O(M_t^4). \quad (25)$$

Here $d_0 = c_0/l_T$.

C. Radiated acoustic power

An analysis, guided by that of Proudman,³ is performed to determine the scaling of the acoustic power per unit mass, P_A , radiated by the turbulence in this problem. Proudman derives

$$P_A \propto \epsilon M_t^5, \quad (26)$$

for sound radiated by a region of isotropic turbulence limited in extent in all three coordinate directions starting from Lighthill's results for the far-field sound radiated by a quadrupole-type source.

For a plane wave, the acoustic intensity, the average rate at which energy is transported across a unit area normal to the propagation direction, is

$$I = \frac{c_0^3 \langle \rho \rangle_{\text{rms}}^2}{\rho_0} = \frac{\langle p \rangle_{\text{rms}}^2}{\rho_0 c_0}. \quad (27)$$

Here $\langle \cdot \rangle_{\text{rms}}$ denotes the root-mean-square (rms) value obtained from the time history of the plane-mean quantity.

As derived in Sec. II for the dipole-type source in this problem

$$\frac{\langle p \rangle_{\text{rms}}}{\rho_0} = O(M_t^3) \quad (28)$$

or

$$\langle p \rangle_{\text{rms}}^2 \propto \rho_0^2 c_0^4 M_t^6. \quad (29)$$

For sound propagating as a plane wave, the radiated acoustic power is

$$P_V = \frac{\langle p \rangle_{\text{rms}}^2 L^2}{\rho_0 c_0} \propto \rho_0 c_0^3 M_t^6 L^2. \quad (30)$$

The total acoustic power per unit mass radiated by a volume of turbulence, $V \sim L^2 l_T$, is

$$P_A = \frac{P_V}{\rho_0 V} \propto \frac{c_0^3 M_t^6}{l_T} \propto \frac{v_T^3 M_t^3}{l_T}. \quad (31)$$

Here l_T is the integral length scale in the propagation direction, and L^2 is the cross-sectional area normal to the direction of plane-wave propagation. Equation (31) can be written in terms of the mean rate of turbulent energy dissipation per unit mass, $\epsilon \sim v_T^3/l_T$

$$P_A \propto \epsilon M_t^3. \quad (32)$$

Equation (32) gives the total acoustic power per unit mass radiated by a dipole-type region of turbulence.

III. NUMERICAL METHODS

A. Governing equations

The equations solved in the DNS are the three-dimensional, compressible, unsteady Navier–Stokes equations written for an ideal, Newtonian fluid. The governing equations are normalized using reference quantities which are denoted by subscript R . Dimensional quantities are denoted by superscript*. The nondimensional density, velocity, and pressure are $\rho = \rho^*/\rho_R$, $\mathbf{u} = \mathbf{u}^*/u_R$, and $p = p^*/p_R$, where $p_R = \rho_R u_R^2$. The nondimensional temperature is T

$=T^*/T_R$, where $T_R = p_R/(\rho_R R_g)$, and R_g is the specific gas constant. Nondimensional length and time are $x = x^*/L_R$, and $t = t^*/t_R$. The equation of state for an ideal gas is $p = \rho T$.

In nondimensional form, the continuity equation is

$$\frac{\partial \rho}{\partial t} + \frac{\partial}{\partial x_i}(\rho u_i) = 0, \quad (33)$$

and the conservative form of the momentum conservation equation is

$$\frac{\partial}{\partial t}(\rho u_i) + \frac{\partial}{\partial x_j}(\rho u_i u_j) = -\frac{1}{\gamma M_R^2} \frac{\partial p}{\partial x_i} + \frac{1}{\text{Re}} \frac{\partial \tau_{ij}}{\partial x_j}, \quad (34)$$

where

$$\tau_{ij} = \mu \left(\frac{\partial u_i}{\partial x_j} + \frac{\partial u_j}{\partial x_i} \right) - \frac{2}{3} \mu \frac{\partial u_k}{\partial x_k} \delta_{ij}. \quad (35)$$

The convective term in the momentum conservation equation is written in the equivalent nonconservative form

$$\frac{\partial}{\partial x_j}(\rho u_i u_j) = \frac{1}{2} \left[u_j \frac{\partial}{\partial x_j}(\rho u_i) + \rho u_i \frac{\partial u_j}{\partial x_j} + \frac{\partial}{\partial x_j}(\rho u_i u_j) \right]. \quad (36)$$

As discussed by Feiereisen *et al.*,¹⁴ discretizing this nonconservative form of the momentum equation using symmetric spatial differences improves the discrete conservation properties of the numerical scheme. The nondimensional energy conservation equation is

$$\begin{aligned} \frac{\partial p}{\partial t} + u_j \frac{\partial p}{\partial x_j} + \gamma p \frac{\partial u_j}{\partial x_j} &= \frac{\gamma}{\text{RePr}} \frac{\partial}{\partial x_j} \left(\kappa \frac{\partial T}{\partial x_j} \right) \\ &+ \frac{\gamma(\gamma-1)M_R^2}{\text{Re}} \Phi, \end{aligned} \quad (37)$$

where

$$\Phi = \tau_{ij} \frac{\partial u_i}{\partial x_j}, \quad (38)$$

is the viscous dissipation function. In Eq. (37), $\text{Pr} = \nu_R/\alpha_R$ is the reference Prandtl number. In Eqs. (34) and (37), $\text{Re} = u_R L_R/\nu_R$ is the reference Reynolds number, and $M_R = u_R/\sqrt{\gamma R_g T_R}$ is the reference Mach number. Here γ is the specific heat ratio, μ_R , ν_R , α_R , and κ_R are the reference dynamic viscosity, kinematic viscosity, thermal diffusivity, and thermal conductivity, respectively. All reference quantities are constant in space and time. The assumption of constant fluid properties is appropriate since the effect of any temperature gradients on the fluid properties is negligible for the low-Mach number flows considered.

B. Discretization

Both first and second spatial derivatives in the x , y , and z directions are calculated using sixth-order compact schemes.¹⁵ The solution is advanced in time using a low-storage, third-order Runge–Kutta scheme.¹⁶ This scheme provides sufficient accuracy while minimizing storage requirements. In the low-storage scheme, only two arrays

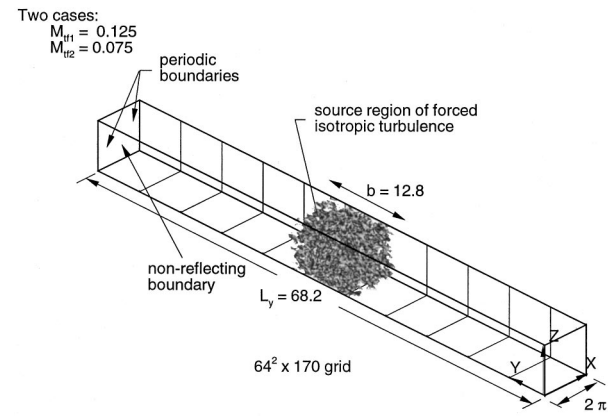


FIG. 1. Schematic of acoustic wave propagation problem for three-dimensional source of forced turbulence.

rather than four are required for each flow-field variable; therefore, the memory required is significantly reduced.

C. Initial condition

The initial source is a region of fully developed, three-dimensional, isotropic turbulence generated in a previous simulation using the algorithm discussed in Sarkar and Hussaini⁴ and used in Whitmire and Sarkar.¹⁷ The algorithm was originally developed to investigate compressibility effects in isotropic turbulence by Erlebacher *et al.*¹⁸ and homogeneous shear turbulence by Sarkar.¹⁹ The initial turbulence has microscale Reynolds number $\text{Re}_\lambda = 34$. The skewness of $\partial u/\partial x$ is -0.45 in the initial field, in agreement with values obtained in previous experiments and simulations of nonlinearly evolving isotropic turbulence. The geometry of the source and acoustic far field is shown in Fig. 1. The turbulence is centered about $y = L_y/2$, where L_y is the length of the computational domain in the y direction.

D. Boundary conditions

Boundary conditions are periodic in the x and z directions and nonreflecting in the y direction. Since the plane-mean sound propagates from the source to the far field in the y direction, truncation of the open physical domain and implementation of nonreflecting boundary conditions is required. The nonreflecting boundary conditions are implemented using the perfectly matched layer (PML) buffer zone technique introduced by Berenger²⁰ for solution of Maxwell's equations in electromagnetics. This technique has been used in fluid dynamic applications by researchers including Hu²¹ and Hayder *et al.*²² In the PML method, the equations solved are designed so that outgoing waves satisfying the linearized Euler equations are damped exponentially to zero in the buffer regions. The PML approach allows use of *periodic* derivative schemes to calculate spatial derivatives in the y direction.

Although these boundary conditions minimize reflections, they do not completely eliminate spurious high-frequency waves. High-frequency oscillations are generated when the pressure waves generated during the initial transient exit boundaries normal to the y direction. A suitably

small hyperviscosity dissipation term is added in the Navier–Stokes equations to damp these high-frequency waves. The hyperviscosity term is proportional to fourth spatial derivatives, and therefore filters any high-frequency oscillations which may contaminate the solution in the interior of the computational domain specifically and strongly. The hyperviscosity term for the conservation equations given in Sec. III A is

$$-\epsilon_E \left(\Delta x^4 \frac{\partial^4 \mathbf{q}}{\partial x^4} + \Delta y^4 \frac{\partial^4 \mathbf{q}}{\partial y^4} + \Delta z^4 \frac{\partial^4 \mathbf{q}}{\partial z^4} \right), \quad (39)$$

where

$$\mathbf{q} = \begin{bmatrix} \rho \\ \rho u \\ \rho v \\ \rho w \\ p \end{bmatrix}. \quad (40)$$

The tunable coefficient, $\epsilon_E = 0.25$, in the hyperviscosity term is chosen to be sufficiently small so that the energy-containing and dissipation ranges are not significantly affected. The damping effect of the hyperviscosity on the turbulence is smaller than that of the physical viscosity for length scales with $l > 2\Delta x$ and is larger than the physical viscosity for smaller length scales. The boundary condition scheme is successful; no significant reflections are observed at the boundaries normal to the y direction.

E. Grid stretching

To resolve the disparate length scales of the turbulence and the acoustic field while minimizing the number of grid points, the grid is stretched in the y direction. The grid is designed so that the spacing is uniform with $\Delta y_{\min} = a$ in the turbulent source, stretched between the source and into the far field, and uniform again with $\Delta y_{\max} = b$ in the far field. The maximum stretch factor, $r = 1.05$, is sufficiently small so that no significant numerical dissipation is introduced by the grid stretching. Here r is the ratio of adjacent intervals between grid points. The grid has uniform spacing, $\Delta x = \Delta z = a$, in the x and z directions. Discretization on a uniform grid which extends to the acoustic far field would require a $64^2 \times 700$ grid containing almost three million grid points instead of the more reasonable $64^2 \times 170$ stretched grid used.

F. Forcing scheme

Preliminary studies show that the amplitude of the plane-mean sound decreases too rapidly to allow statistical analysis for the case where the source is a region of decaying turbulence. A unique forcing scheme is devised to maintain energy in the turbulence so that predictions of the Lighthill acoustic analogy for the statistics of the plane-mean sound can be evaluated. In this forcing scheme, an energy spectrum typical of fully developed isotropic turbulence is maintained. The turbulence is forced so that the source turbulent Mach number is constant in time (after an initial transient). No significant dilatation (larger amplitude “monopole-type”

sound) is introduced by the forcing method; therefore, spurious noise that would dominate the predicted dipole-type sound is avoided.

A region of forced turbulence which meets these requirements is obtained by forcing the incompressible component of the velocity field, \mathbf{u}^I , so that the incompressible energy spectrum is invariant with time for a range of forced wave numbers. The velocity field can be decomposed into two components, $\mathbf{u} = \mathbf{u}^I + \mathbf{u}^C$, where the incompressible component, \mathbf{u}^I , is solenoidal and contains all the vorticity

$$\nabla \cdot \mathbf{u}^I = 0, \quad \nabla \times \mathbf{u}^I = \nabla \times \mathbf{u}, \quad (41)$$

and the compressible component, \mathbf{u}^C , contains all the dilatation but none of the vorticity,

$$\nabla \cdot \mathbf{u}^C = \nabla \cdot \mathbf{u}, \quad \nabla \times \mathbf{u}^C = 0. \quad (42)$$

To avoid the introduction of significant dilatation, \mathbf{u}^C is not forced. Only the incompressible velocity component, \mathbf{u}^I , is forced. The range of forced wave numbers is $k_{\min} \leq k_r \leq k_{\max}$. Here $k_{\min} = 4$, $k_{\max} = 12$, and k_r is the radial wave number. In this forcing scheme, the low-wave number scales of the flow that are frequency matched with the far-field sound are not forced directly since $k_{\min} > k_A = \omega/c_0$.

Two computational grids are required to efficiently implement the forcing scheme. One grid is the stretched grid described in Sec. III E. This stretched grid contains $64^2 \times 170$ points and extends from the turbulence to the acoustic far field. The second grid is a smaller uniform grid containing $64^2 \times 128$ points with spacing $\Delta x = \Delta y = \Delta z = 2\pi/64$. The uniform spacing on the smaller grid is the same as the uniform spacing in the turbulence on the larger stretched grid. The smaller grid contains the entire turbulent source.

The incompressible velocity field is forced at the end of each time step. The total velocity field is first transferred from the stretched to the smaller uniform grid, $\mathbf{u} \rightarrow \mathbf{u}^*$. The velocity field on the smaller grid is truncated and damped so $\mathbf{u}^* \rightarrow 0$ at the boundaries normal to the y direction to obtain the periodic boundary conditions required to perform Fourier transforms in y . The total velocity field on the smaller uniform grid is then transformed into spectral space, $\mathbf{u}^* \rightarrow \widehat{\mathbf{u}}^*$, and decomposed into its incompressible and compressible parts, $\widehat{\mathbf{u}}^* \rightarrow \widehat{\mathbf{u}}^{*I} + \widehat{\mathbf{u}}^{*C}$. The incompressible velocity field is forced, $\widehat{\mathbf{u}}^{*I}(k_r) \rightarrow \widehat{\mathbf{u}}^{*I}_F(k_r)$. At the end of each time step, $\widehat{\mathbf{u}}^{*I}(k_r)$ with k_r in the range of forced wave numbers is multiplied by a constant $\beta(t)$. The value of β is determined from the condition that the turbulent kinetic energy must be the same at the beginning and end of each time step. Thus, the energy lost due to viscous dissipation is replenished by the forcing. The forced and unforced incompressible velocity fields, $\widehat{\mathbf{u}}^{*I}_F$ and $\widehat{\mathbf{u}}^{*I}$, are then transformed from spectral to physical space and transferred to the larger stretched grid. The total velocity field in physical space is calculated as $\mathbf{u} = \mathbf{u}^C + \mathbf{u}^I_F$. Note that \mathbf{u}^C is not altered by the forcing scheme; no spurious dilatation is introduced.

The unique forcing scheme developed and implemented is extremely successful. For each of the two cases considered, the source turbulent Mach number after the initial transient, M_{tf} , is constant in time. No significant dilatation is

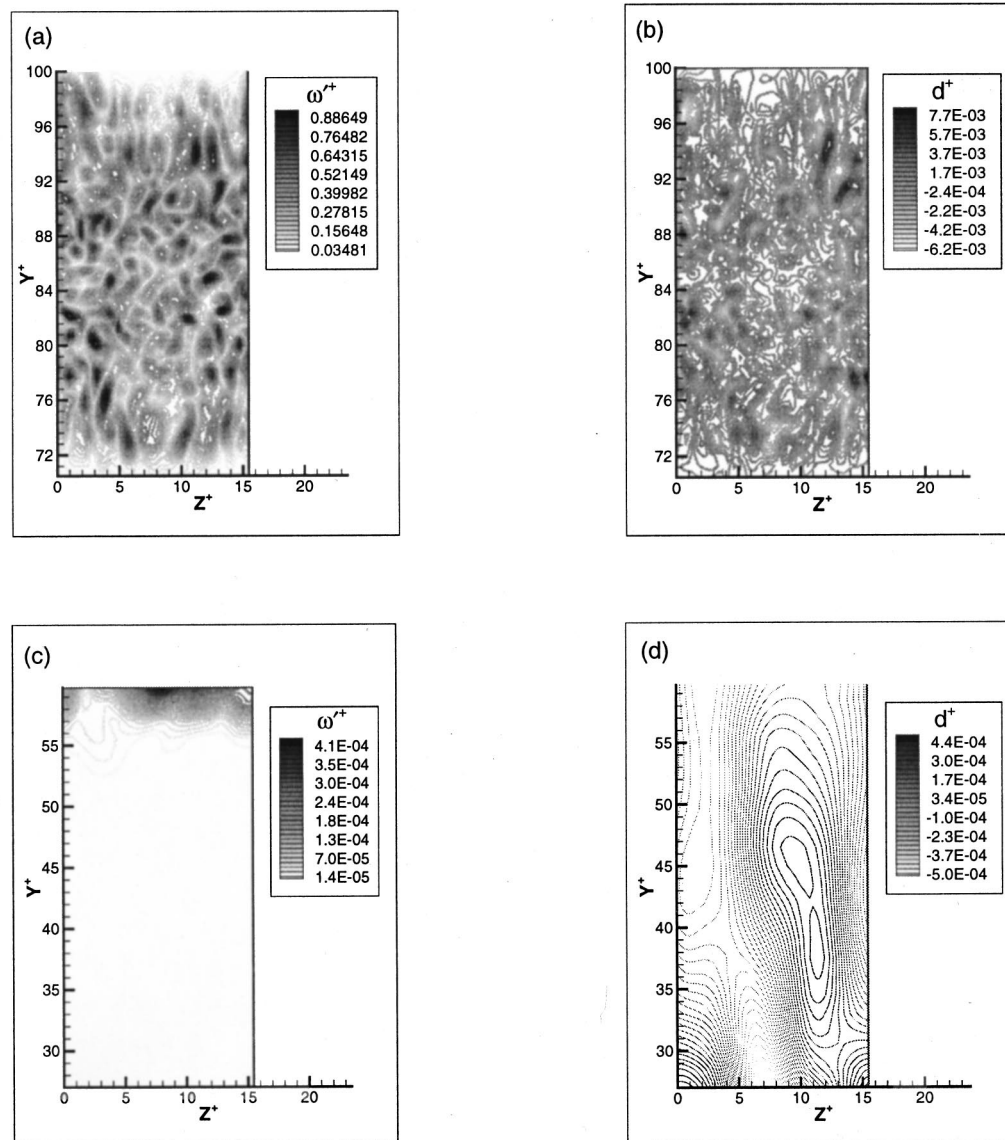


FIG. 2. Contours of vorticity magnitude and dilatation fluctuations generated by a three-dimensional region of forced turbulence. All figures give instantaneous levels at $t^+ = 338$ for $M_{tf1} = 0.125$. (a) and (b) are in the turbulence, and (c) and (d) are in the acoustic far field. In (c) and (d), the sound is propagating downward towards $y^+ = 0$. The computational domain extends from $y^+ = 0$ to $y^+ = L_y^+ = 171$, and the turbulence is centered about $y^+ = L_y^+/2$.

introduced either through the two interpolations between the stretched and uniform grids or during the forcing

IV. NUMERICAL RESULTS

A. DNS results for the flow evolution

The two cases considered have turbulent Mach numbers $M_{tf1} = 0.125$ and $M_{tf2} = 0.075$. Here the subscript f is used to denote final, steady values after the initial transient. Each of the two cases requires 30 MW of memory and 150 CPU hours on the Cray C-90. In each case, the solution of the three-dimensional, compressible Navier–Stokes equations is computed for 8200 time intervals of $\Delta t = 0.0072$, and a time series of length nT_A with $n = 35$ is used to evaluate the statistics of the turbulence and the sound. Here n is the number of time periods for each case, and T_A is the length of a single time period. The time period of both the turbulence and the

sound scales as the eddy turnover time; $n_1 \approx 8$ for the case with $M_{tf1} = 0.125$, and $n_2 \approx 5$ for the case with $M_{tf2} = 0.075$. The acoustic wavelength is resolved with a minimum of 10 points per wavelength. In this section, nondimensional variables are as defined in Sec. III A. In Figs. 2–8, the vorticity, dilatation, velocity, length, time, and frequency as defined in Sec. III A are further normalized using length scale l_T and velocity scale c_0 . These normalized quantities are $\omega^+ = \omega/(c_0/l_T)$, $d^+ = d/(c_0/l_T)$, $v^+ = v/c_0$, $Y^+ = y/l_T$, and $Z^+ = z/l_T$, $t^+ = t/(l_T/c_0)$, and $f^+ = f/(c_0/l_T)$.

Figure 2 shows contours of fluctuating vorticity, ω' , and dilatation, d , in the turbulence and acoustic far field at time $t^+ = 338$ after the initial transient has exited the computational domain. Figures 2(a) and 2(b) are in the turbulence, and Figs. 2(c) and 2(d) are in the acoustic far field. The figures shown are for the case with $M_{tf1} = 0.125$. Contours are qualitatively the same for the case with $M_{tf2} = 0.075$.

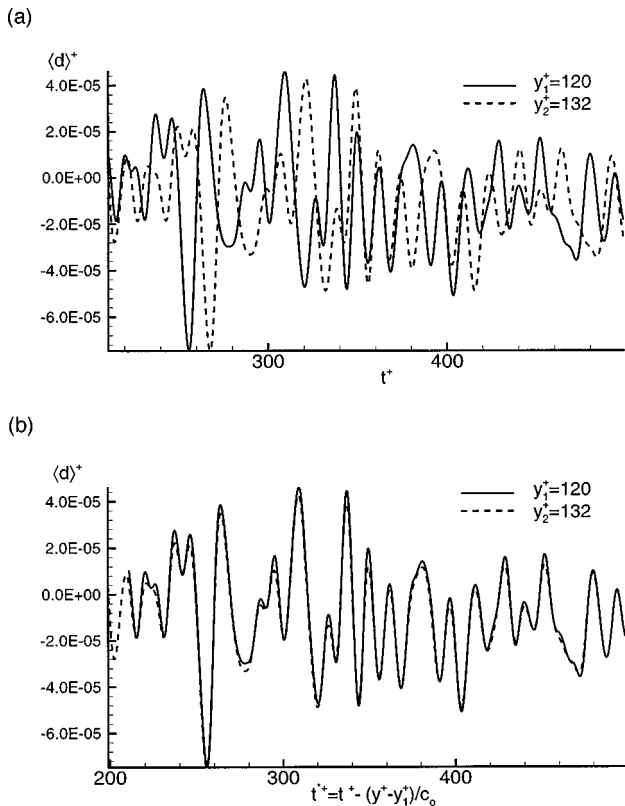


FIG. 3. Time evolution of plane-mean dilatation fluctuations at two different observation planes in the acoustic far field for $M_{t,f1} = 0.125$ (a) curves not shifted in time (b) curve at $y_2 > y_1$ shifted by d/c_0 , where $d = y_2 - y_1$.

During the initial transient, the turbulence spreads in time as $b \sim \sqrt{\nu_T t}$, where $\nu_T \sim l_T \nu_T$ is the eddy viscosity. As discussed in Sec. III F, the dimension of the turbulence in the y direction is constrained to be no larger than the dimension of the smaller grid used to force the turbulence. After the initial transient, the extent of the turbulence in the y direction is $b^+ = b/l_T = 32$. The turbulence is decorrelated in x , y , and z . Integral length scales in the x , y , and z directions are $l_x \approx l_y \approx l_z \approx 0.4$. The ratio of the integral length scale to the extent of the turbulence in the x , y , and z directions is $l_x/L \approx 0.06$, $l_y/b \approx 0.03$, and $l_z/L \approx 0.06$. Here $L = L_x = L_z$ is the dimension of the computational domain in the x and z directions. The Taylor microscale is $\lambda^+ = \lambda/l_T \approx 0.35$. Here $l_T \approx l_x, l_y, l_z$. The magnitude of all components of the Rey-

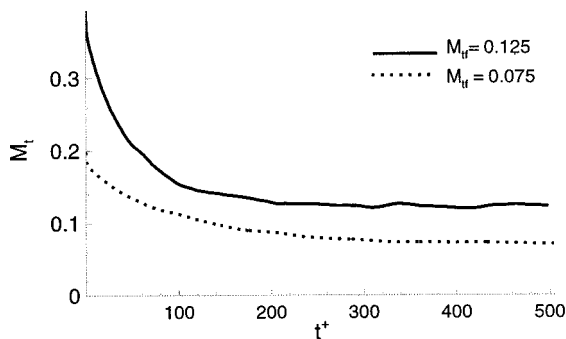


FIG. 4. Time evolution of turbulent Mach number in three-dimensional source of forced turbulence.

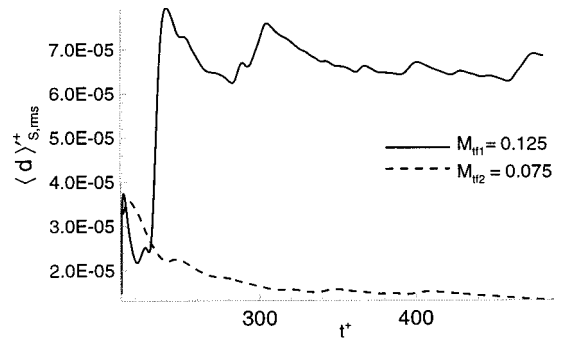


FIG. 5. Time-rms plane-mean dilatation in the turbulent source.

nolds stress anisotropy, b_{ij} , is less than 0.02 in the core of the turbulent source and increases to 0.1 near the source boundaries normal to the y direction. Because of the isotropic forcing scheme used, the turbulence does not deviate much from isotropy.

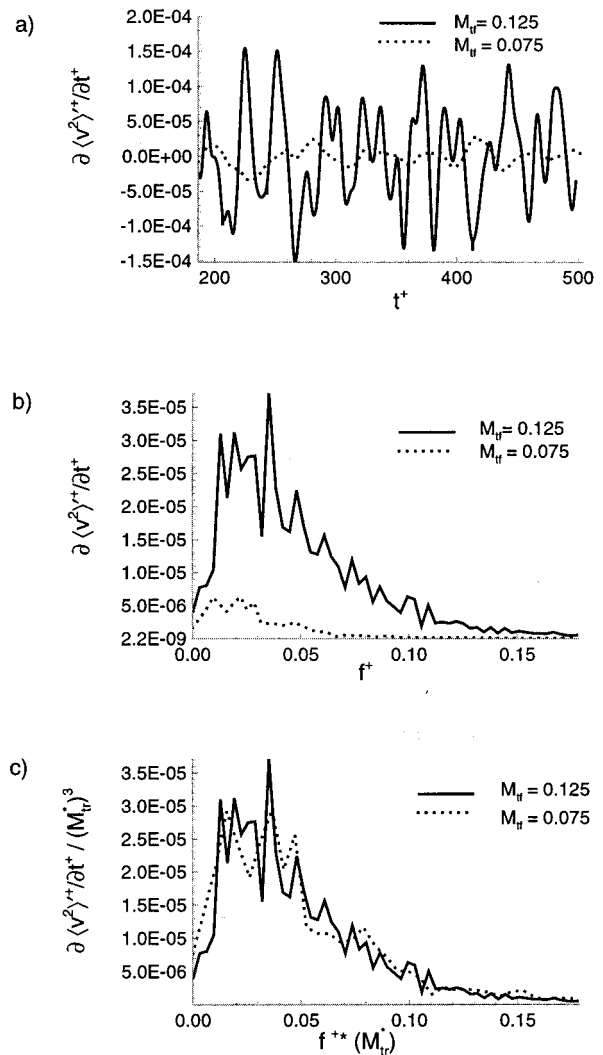


FIG. 6. Lighthill acoustic analogy plane-mean source term in three-dimensional, bounded region of forced turbulence: (a) Time history (b) Fourier transform in time (unscaled) (c) Fourier transform in time (normalized using acoustic-analogy predictions). Here $M_{tr}^* = M_{t,f1} / M_{t,f}$.

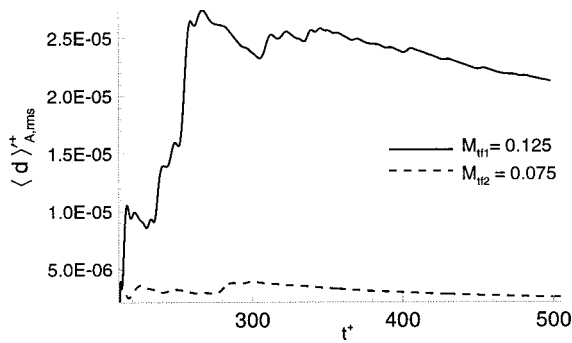


FIG. 7. Time-rms plane-mean dilatation in the acoustic far field.

Although the incompressible field in the turbulence is constrained in the y direction, the compressible field has no such constraints. The acoustic wavelength is determined by the requirement, $k_A = \omega/c_0$. The ratio l_T/λ_A for the cases with $M_{tf1} = 0.125$ and $M_{tf2} = 0.075$ is 0.044 and 0.028, respectively. Since $l_T/\lambda_A \ll 1$, the source is spatially compact. The two buffer regions used to implement the nonreflecting boundary conditions extend from $y^+ = 0-27$ and $y^+ = 144-171$. These buffer regions are not shown in Fig. 2. As shown in Fig. 2(c), vorticity fluctuations are essentially zero outside the turbulence. Figure 2(d) shows that the acoustic fluctuations propagate to the far field. The increase in length scales from the turbulence to the acoustic far field can be seen by comparing Figs. 2(b) and 2(d).

Figure 3(a) shows the time evolution of the plane-mean dilatation at two planes in the acoustic far field for the case with $M_{tf1} = 0.125$. Figure 3(b) shows the curves in Fig. 3(a) with the curve for $y_2 > y_1$ shifted by d/c_0 where d is the distance in the y direction between the two planes. As shown in these figures, the plane-mean sound propagates as a plane wave from the turbulence to the acoustic far field. The amplitude of the far-field, plane-mean sound is not a function of y for this case with one-dimensional wave propagation. Both the shape and amplitude of the plane-mean sound are nearly identical (but shifted in time by d/c_0) at different planes in the acoustic far field. The result that the sound waves travel with the speed of sound indicates that spurious numerical dispersion is insignificant. The transition from the near field to the far field is identified as the location where the shape and amplitude of the plane-mean sound become nearly identical at various observation planes. This occurs at $y/\lambda_A \approx 0.5$. Figures 3(a) and 3(b) also show that no significant reflections in the plane-mean sound are generated at the non-reflecting boundaries. For $t^+ > 59$, any reflections from the domain exit would have propagated into the test region and would be seen as differences in the shape and amplitude of the plane-mean sound at different planes.

Figure 4 shows the time evolution of the source turbulent Mach number for the two simulations. After an initial transient, the turbulent Mach number for each case and, therefore, the turbulent Mach number ratio, $M_{tr} = M_{tf1}/M_{tf2} = 1.67$, is constant in time. The decrease in M_{tr} to its final steady value during the initial transient is due to the increase in the volume of the turbulent region; the total kinetic energy in the turbulent region with volume $V(t)$

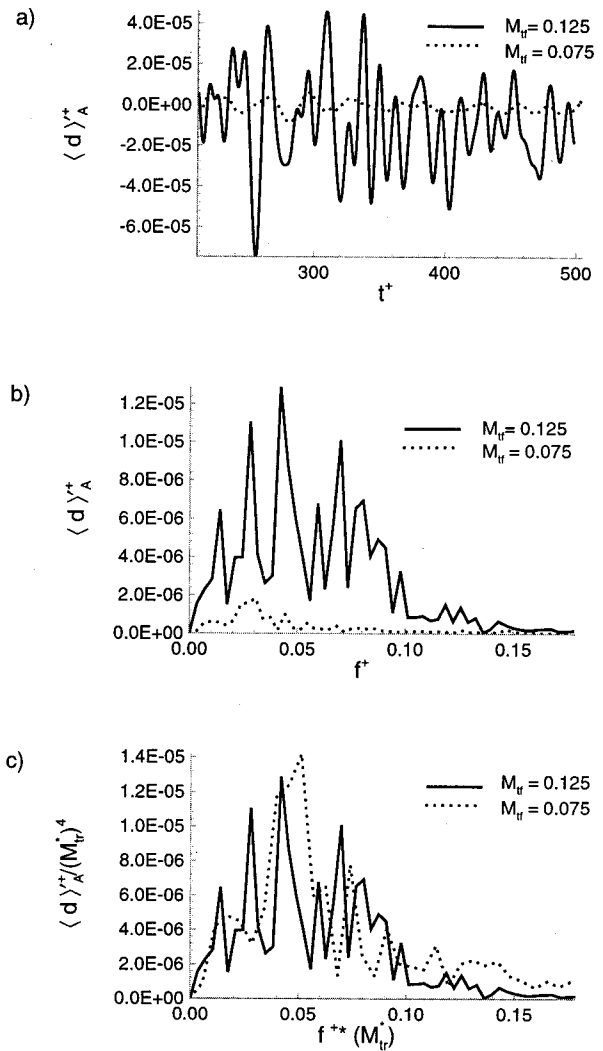


FIG. 8. Plane-mean dilatation in acoustic far field generated by three-dimensional, bounded region of forced turbulence: (a) Time history (b) Fourier transform in time (unscaled) (c) Fourier transform in time (normalized using acoustic-analogy predictions). Here $M_{tr}^* = M_{tf1}/M_{tf2}$.

$= L^2 b(t)$ is constant in time both during and after the initial transient.

B. Comparison of acoustic-analogy predictions with DNS results

1. Evaluation of scaling predictions for Lighthill source term in turbulence

Figure 5 shows the time-rms plane-mean dilatation, $\langle d \rangle'_{S,rms}$ in the turbulent source for the two DNS cases. The time-rms dilatation is calculated as a running average

$$\langle d \rangle'_{rms}(t) = \sqrt{\frac{1}{t} \int_{t=25}^t \langle d \rangle'(y,t) dt}. \tag{43}$$

After an initial transient, $\langle d \rangle'_{S,rms}$ is constant for each case. To check the prediction of Eq. (24) for the scaling of dilatation fluctuations in the turbulence, $\langle d \rangle'_S/d_0 = O(M_t^2)$, the scaling exponent defined as

$$x_S = \frac{\ln(\langle d \rangle'_{S1,rms} / \langle d \rangle'_{S2,rms})}{\ln(M_{tf1} / M_{tf2})}, \quad (44)$$

is determined from the curves in Fig. 5. Analysis predicts $x_S = 3.0$, and DNS results give $x_S = 3.1$. Agreement between the analysis and the DNS results is good. Note that the time-rms quantities include contributions from the many frequencies present in the turbulence.

Figure 6 shows the time evolution of $\partial \langle v^2 \rangle' / \partial t$ for the two DNS cases. A range of frequencies with varying amplitudes are present in the turbulence. The time series for the case with the higher M_{tf} has higher fluctuation amplitude and contains a wider range of frequencies. To quantify these observations, the Fourier transform in time of $\partial \langle v^2 \rangle' / \partial t$ is obtained for each case. Plots of the Fourier transform of the source term, $\partial \langle \widehat{v^2} \rangle' / \partial t(y, f)$, as a function of frequency, f , are shown in Fig. 6(b). Each curve shown is an average of the Fourier transforms at five planes in the turbulent source. Figure 6(b) shows that a range of frequencies with varying amplitudes are present in the Lighthill source term. The amplitude of $\partial \langle v^2 \rangle' / \partial t$ is larger for all frequencies for the case with higher M_{tf} . The dominant frequency is higher for the case with $M_{tf1} = 0.125$ compared to the case with $M_{tf2} = 0.075$.

Figure 6(c) shows the curves in Fig. 6(b) normalized using the predicted scaling with turbulent Mach number. The normalized amplitude is $\partial \langle \widehat{v^2} \rangle' / \partial t / M_{tr}^{*3}$, and the normalized frequency is $f M_{tr}^*$. Here $M_{tr}^* = M_{tf1} / M_{tf}$ is $M_{tr}^* = 1.67$ for the case with $M_{tf2} = 0.075$ and $M_{tr}^* = 1.00$ for the case with $M_{tf1} = 0.125$. The normalization collapses the spectra as shown in Fig. 6(c), indicating the validity of the analytical predictions that the frequency of the source term scales as M_t , and the amplitude scales as M_t^3 .

2. Evaluation of scaling predictions for the radiated far-field sound

Figure 7 shows the time-rms plane-mean dilatation, $\langle d \rangle'_{A,rms}$, at a plane in the acoustic far field for the two DNS cases. The time-rms value is calculated as in the turbulent source using the definition in Eq. (43). After an initial transient, $\langle d \rangle'_{A,rms}$ is constant in time. To check the prediction given by Eq. (25) for the scaling of dilatation fluctuations in the far field, $\langle d \rangle'_A / d_0 = O(M_t^4)$, the scaling exponent defined as

$$x_A = \frac{\ln(\langle d \rangle'_{A1,rms} / \langle d \rangle'_{A2,rms})}{\ln(M_{tf1} / M_{tf2})}, \quad (45)$$

is determined from the curves in Fig. 7. Analysis predicts $x_A = 4.0$, and DNS results give $x_A = 4.2$. Agreement between the DNS results and the acoustic-analogy predictions is good.

Figure 8(a) shows the time evolution of $\langle d \rangle'_A$ at a plane in the acoustic far field. The Fourier transform in time of the far-field sound, $\langle \widehat{d} \rangle'_A(y, f)$, as a function of f is shown in Fig. 8(b). Almost identical spectra are obtained at any plane in the far field since both the amplitude and shape of the plane-mean sound are nearly identical (but shifted) at different planes. Figure 8(b) shows that a range of frequencies with

varying amplitudes are present in the plane-mean sound. The amplitude of $\langle d \rangle'_A$ is larger for all frequencies for the case with higher M_{tf} . The dominant frequency is also higher for the case with $M_{tf1} = 0.125$ compared to the case with $M_{tf2} = 0.075$.

Figure 8(c) shows the curves in Fig. 8(b) normalized using predictions of the Lighthill acoustic analogy for the scaling of the amplitude and frequency of the far-field, plane-mean sound with turbulent Mach number. The normalized amplitude is $\langle \widehat{d} \rangle'_A / M_{tr}^{*4}$, and the normalized frequency is $f M_{tr}^*$. As predicted by the Lighthill acoustic analogy, this normalization collapses the spectra as shown in Fig. 8(c), indicating the validity of the analytical predictions that the frequency of the plane-mean sound scales as M_t , and the amplitude scales as M_t^4 for a range of frequencies.

3. Evaluation of scaling predictions for radiated acoustic power

The predicted scaling of the radiated acoustic power derived in Sec. II C for a dipole-type source, $P_A \propto \epsilon M_t^3$, [Eq. (32)] is evaluated using the DNS results. Combining Eqs. (30) and (32), the acoustic power per unit mass of the turbulent source is

$$P_A = \alpha_\epsilon \epsilon M_t^3 = \frac{\langle p \rangle_{rms}^2}{\rho_0^2 c_0^2 l_T}, \quad (46)$$

where α_ϵ is a constant independent of turbulent Mach number. The right-hand-side of Eq. (46) is rewritten in terms of $\langle d \rangle_{rms}$ instead of $\langle p \rangle_{rms}$ because, as discussed in Sec. II B, the low-frequency drift in the mean pressure complicates the computation of $\langle p \rangle_{rms}$. So, Eq. (46) becomes

$$P_A \propto \frac{\langle d \rangle_{rms}^2 c_0^3 l_T}{V_T^2}. \quad (47)$$

To check the predicted scaling of the radiated acoustic power for a dipole-type source of turbulence, the ratio $\alpha_{\epsilon 1} / \alpha_{\epsilon 2}$ is evaluated using the DNS results. Here $\alpha_{\epsilon 1}$ and $\alpha_{\epsilon 2}$ are the proportionality constants for the cases with $M_{tf1} = 0.125$ and $M_{tf2} = 0.075$, respectively. From the DNS results

$$\frac{\alpha_{\epsilon 1}}{\alpha_{\epsilon 2}} = 1.2. \quad (48)$$

Thus, the quantity α_ϵ does not vary significantly with turbulent Mach number in the DNS. These results verify the predicted scaling of the radiated acoustic power per unit mass, $P_A \propto \epsilon M_t^3$, for a dipole-type source.

V. CONCLUSIONS

The ability of the Lighthill acoustic analogy to predict the sound radiated by a three-dimensional region of turbulence is evaluated by comparing DNS results with acoustic-analogy predictions. In the DNS, the three-dimensional, unsteady, compressible Navier–Stokes equations are solved on a large computational domain which includes the turbulence and extends to the acoustic far field. The turbulence is limited in extent in one coordinate direction and is periodic in

the other two directions. An analysis based on Lighthill's acoustic analogy shows that the turbulent region considered in this problem is a dipole-type source; the rms pressure, rms dilatation, and peak acoustic frequency are predicted to scale as M_t^3 , M_t^4 , and M_t , respectively. Agreement between the DNS results and the acoustic-analogy predictions is good. DNS results also confirm that the radiated acoustic power per unit mass scales as $P_A \propto \epsilon M_t^3$ as derived for a dipole-type source. Note that turbulent flows most often are a combination of multipoles of different order; acoustic-analogy validation using experimental data is more difficult than the validation using DNS results performed here.

Results show that critical numerical issues are resolved appropriately in the DNS. The computational domain is stretched in the direction of sound propagation to minimize the number of grid points required. Nonreflecting boundary conditions are implemented without introducing any significant reflections in the sound even though the acoustic density fluctuation normalized by the mean density is $O(10^{-4})$. Forcing the turbulence without introducing larger amplitude monopole-type sound is a significant challenge. A unique forcing scheme is developed to force the incompressible velocity field without forcing the compressible velocity field in order to maintain an energy spectrum typical of fully developed turbulence. Finally, applying the Lighthill acoustic analogy is not trivial. Careful evaluation of the appropriate source term in the acoustic analogy is essential to the prediction of the dipole-type sound observed here.

A DNS which includes both the turbulence and the acoustic far field is computationally expensive and problematic, even for the simple problem considered here. In fact, the difficulty and cost of implementing full DNS to calculate the far-field sound convincingly demonstrates the advantages of a hybrid approach. This study validates predictions of the Lighthill acoustic analogy for sound radiated by three-dimensional, broadband turbulence.

ACKNOWLEDGMENTS

This study was partially supported by the National Aeronautics and Space Administration (NASA) through NASA Grant No. NAG-1-1535. Supercomputer time was provided by the Numerical Aerospace Simulation Facility (NAS) at NASA Ames Research Center and by the San Diego Supercomputer Center (SDSC).

- ¹D. G. Crighton, "Basic principles of aerodynamic noise generation," *Prog. Aerosp. Sci.* **16**, 31 (1975).
- ²M. J. Lighthill, "On sound generated aerodynamically. I. General theory," *Proc. R. Soc. London, Ser. A* **211**, 564 (1952).
- ³I. Proudman, "The generation of noise by isotropic turbulence," *Proc. R. Soc. London, Ser. A* **214**, 119 (1952).
- ⁴S. Sarkar and M. Y. Hussaini, "Computation of the sound generated by isotropic turbulence," ICASE Report 93-74 (1993).
- ⁵A. Witkowska, J. G. Brasseur, and D. Juve, "Numerical study of noise from stationary isotropic turbulence," AIAA Pap. 95-037 (1995).
- ⁶G. M. Lilley, "The radiated noise from isotropic turbulence," *Theor. Comput. Fluid Dyn.* **6**, 281 (1994).
- ⁷T. Dubois, Private communication referenced in Lilley (Ref. 6) (1993); Also see A. Debussche, T. Dubois, and R. Teman, "The nonlinear Galerkin method: A multi-scale method applied to the simulation of homogeneous turbulent flows," ICASE Report 93-93 (1993).
- ⁸B. E. Mitchell, S. K. Lele, and P. Moin, "Direct computation of sound from a compressible co-rotating vortex pair," AIAA Pap., Pap. 92-0374 (1992).
- ⁹T. Colonius, S. K. Lele, and P. Moin, "The scattering of sound waves by a vortex: numerical simulations and analytical solutions," *J. Fluid Mech.* **206**, 271 (1994).
- ¹⁰T. Colonius, P. Moin, and S. K. Lele, "Direct computation of aerodynamic sound," Report TF-65 Thermosciences Division, Department of Mech. Engineering, Stanford University (1995).
- ¹¹B. E. Mitchell, S. K. Lele, and P. Moin, "Direct computation of the sound generated by subsonic and supersonic axisymmetric jets," Report TF-66 Thermosciences Division, Department of Mech. Engineering, Stanford University (1995).
- ¹²F. Bastin, P. Lafon, and S. Candel, "Computation of jet mixing noise due to coherent structures: the plane jet case," *J. Fluid Mech.* **11**, 1 (1995).
- ¹³J. B. Freund, "Acoustic Sources in A Turbulent Jet: A Direct Numerical Simulation Study," AIAA Pap., Pap. 99-1858 (1999).
- ¹⁴W. J. Feiereisen, W. C. Reynolds, and J. H. Ferziger, "Simulation of a Compressible Homogeneous Turbulent Shear Flow," Report TF-13, Department of Mech. Engineering, Stanford University (1995).
- ¹⁵S. K. Lele, "Compact finite difference schemes with spectral-like resolution," *J. Comput. Phys.* **103**, 16 (1992).
- ¹⁶J. H. Williamson, "Low-storage Runge-Kutta schemes," *J. Comput. Phys.* **35**, 48 (1980).
- ¹⁷J. Whitmire and S. Sarkar, "The computation of flow-generated sound using an acoustic analogy," AIAA Pap., Pap. 95-038 (1995).
- ¹⁸G. Erlebacher, M. Y. Hussaini, H. O. Kreiss, and S. Sarkar, "The analysis and simulation of compressible turbulence," *Theor. Comput. Fluid Dyn.* **2**, 73 (1990).
- ¹⁹S. Sarkar, "The stabilizing effect of compressibility in turbulent shear flow," *J. Fluid Mech.* **282**, 163 (1995).
- ²⁰J.-P. Berenger, "A Perfectly Matched Layer for the absorption of electromagnetic waves," *J. Comput. Phys.* **114**, 185 (1994).
- ²¹F. Q. Hu, "On absorbing boundary conditions for linearized Euler equations by a Perfectly Matched Layer," *J. Comput. Phys.* **129**, 201 (1996).
- ²²M. E. Hayder, F. Q. Hu, and M. Y. Hussaini, "Towards perfectly absorbing boundary conditions for Euler equations," ICASE Report 97-25 (1997).